Can Hyperscale Data Centers Alter Local Meteorology in the Kathmandu Valley? A Simulation-Based Assessment

Sujan Bhattarai[1], Saroj Prasad Mainali[2], Suman Bhattarai[2]

Affiliations:

[1] The Small Earth Nepal, Kathmandu, Nepal
[2] Institute of Engineering, Thapathali Campus, Tribhuvan University, Kathmandu, Nepal

Corresponding author: Sujan Bhattarai, Email: sujanbhattarai.jr@gmail.com

Abstract

There is growing interest in Nepal in hosting large data centers inside the Kathmandu Valley, but how the valley's atmosphere would respond to substantial additional heat emissions remains uncertain. The Kathmandu Valley is a closed bowl-shaped basin surrounded by mountains, with persistent nocturnal cold pools and weak boundary-layer winds that limit the dispersal of pollutants and heat from the basin. These features make it a difficult receiving environment for a large data center, whose operation produces huge quantities of waste heat that must be released into the local atmosphere. This study presents a scientific assessment of whether siting such a facility in the valley would cause measurable temperature changes in the city, intended to scientifically inform the ongoing public discussion. We use publicly available satellite and reanalysis datasets, including ERA5-Land, MODIS, Sentinel-2, ESA WorldCover, GHSL built-up, and SRTM elevation data, to estimate the additional heat that a hypothetical 50, 150, or 500 megawatt data center would inject into the valley atmosphere if placed on the southern valley floor. The analytical results show that the temperature impact during daytime would be small, because afternoon up-valley winds advect the heat plume away from the urban core. At night, however, drainage flow reverses the wind direction and carries the plume toward central Kathmandu, raising local temperatures by approximately 0.1 to 0.5 °C for a medium-sized facility and 0.4 to 2.0 °C for a very large one. Based on these results, a small data center on the order of 50 megawatts is of limited meteorological concern under the valley's regime, while larger facilities produce a temperature signature that becomes measurable at the urban core. While this study evaluates atmospheric implications, the broader environmental feasibility of hyperscale data-center deployment depends heavily on freshwater use and wastewater management. It remains unclear how such demand, along with cooling-related

wastewater discharge, would be managed. These hydrological implications therefore require dedicated assessment before any large-scale data-center development is approved.

Keywords: data center; anthropogenic heat flux; urban heat island; Kathmandu Valley; meteorology; AI infrastructure

1. Introduction

Global data center capacity is undergoing the largest infrastructure build-out of the digital era. Synergy Research Group reports that the total number of hyperscale data centers passed 1,000 in 2024 and continues to grow at roughly 130 new facilities per year, with average per-facility critical IT capacity rising sharply due to AI training and inference workloads (Synergy Research Group, 2024). Whereas a typical traditional cloud data center has historically been sized at 25 to 30 MW (Morgan, 2014), single-campus designs in the 100 to 500 MW range are now routine in announced AI-focused builds, and projects exceeding 1 GW are under active development (MMCG Invest, 2026).

Most published environmental analyses of data centers have focused on annual carbon emissions and aggregate national-scale resource demand (Attenni et al., 2026; Lawson et al., 2026; Turkay et al., 2026). Comparatively little work has examined the local meteorological footprint at the scale of a single facility, yet the physics of waste-heat injection makes locality the relevant scale: roughly 100 percent of electrical energy delivered to IT equipment leaves the campus as low-grade heat, partitioned between sensible exhaust and latent heat from evaporative cooling (Sailor, 2011). For a 150 MW facility on a 20-hectare footprint operating at a typical hyperscale Power Usage Effectiveness (PUE) of 1.3, this corresponds to a campus-mean anthropogenic heat flux of order 1,000 W m^{-2}, roughly an order of magnitude greater than anthropogenic heat fluxes for the densest central business districts of major Asian cities (Hu et al., 2012; Chen & Hu, 2017). When that flux is concentrated in a single grid cell of a mesoscale model rather than distributed across an urban canopy, the resulting forcing has more in common with a small power station than with a piece of urban land use.

The receiving environment matters as much as the source. The Kathmandu Valley is a closed bowl-shaped basin of ~340 km^2 floor area at 1,300 m elevation, surrounded by ridges rising to 2,000 to 2,800 m, with one narrow river outlet to the south. Its meteorology is dominated by a strong diurnal valley-mountain wind cycle: daytime up-valley flow that ventilates the basin via lateral mountain passes,

and nocturnal drainage of cold air from the surrounding slopes that produces a deep stable cold pool over the valley floor, with mixing heights collapsing to a few hundred meters (Regmi et al., 2003; Mues et al., 2017). This regime is responsible for the city's persistent winter and pre-monsoon air-quality crises, in which temperature inversions trap fine particulate matter at the surface and produce some of the highest PM2.5 concentrations recorded in any capital city (Shakya et al., 2017; Saud & Paudel, 2018; IQAir, 2023). The same ventilation-limited regime that traps pollution would also trap any local heat source.

There is growing public and policy interest in Nepal in hosting large data centers inside the Kathmandu Valley, motivated by the global expansion of AI compute infrastructure and the prospect of regional digital-economy participation. To our knowledge, no prior study has quantified the meteorological footprint of a hypothetical data center in a Himalayan valley city. This paper develops such a framework and reports analytical-model results. The objective is to provide a quantitative atmospheric baseline against which the current siting discussion can be evaluated.

We address two questions:

(1) What is the magnitude and spatial scale of the near-surface temperature anomaly caused by a 50, 150, or 500 MW data center on the southern Kathmandu Valley floor, under representative day and night atmospheric regimes?

(2) How do these temperature impacts compare with the existing meteorological heterogeneity of the city, and at what facility size do they become a meteorological concern?

Data-center impacts are most heavily on the regional water system, while this study focuses only on atmospheric implications. Future studies should therefore investigate cooling-related wastewater management, hydrological impacts, and potential effects on river morphology and freshwater biodiversity before large-scale facility deployment is considered.

2. Study Area

The Kathmandu Valley (27.4 to 27.8° N, 85.2 to 85.6° E; valley-floor elevation ~1,300 to 1,400 m a.s.l.) lies between the Lesser and Greater Himalaya in central Nepal and contains the Kathmandu, Lalitpur, and Bhaktapur metropolitan areas, with a combined population of approximately 3 million. The valley is a near-closed basin: its floor is encircled by ridges of 2,000 to 2,800 m, broken by five mountain passes

between 1,500 and 1,550 m and a single narrow river outlet, the Bagmati River gorge, draining to the south (Panday & Prinn, 2009). The vertical relief to horizontal extent ratio is approximately 1:30.

The valley climate is characterized by a five-season monsoonal regime (Mahata et al., 2017), with the dry pre-monsoon period (March to May) historically registering the strongest atmospheric stagnation and the highest PM2.5 concentrations (IQAir, 2023). Long-term observations reveal a consistent diurnal cycle in which up-valley flow develops shortly after midday and intrudes the basin through the western and southwestern passes (Regmi et al., 2003), while at night radiative cooling and slope-driven drainage establish a deep cold pool over the valley floor with surface inversions persisting from sunset to ~07:00 LT (Mues et al., 2017).

The hypothetical data center site for this study is located at 27.620° N, 85.310° E, approximately 12 km south of central Kathmandu on the Lalitpur to southern-rim transition (Figure 1). Site selection reflects three considerations: (i) the location is on the valley floor at an elevation similar to that of central Kathmandu, eliminating elevation as a confounding factor in plume calculations; (ii) it sits south of the urban core, so under the prevailing daytime up-valley wind regime the heat plume is advected away from the city; and (iii) under the nocturnal drainage regime, the same site is upwind of the urban core, allowing the plume to interact with the city's stable nocturnal boundary layer. This configuration provides the strongest contrast in day-night exposure between the two regimes and therefore the cleanest test case for the hypothesis that valley meteorology controls the local impact.

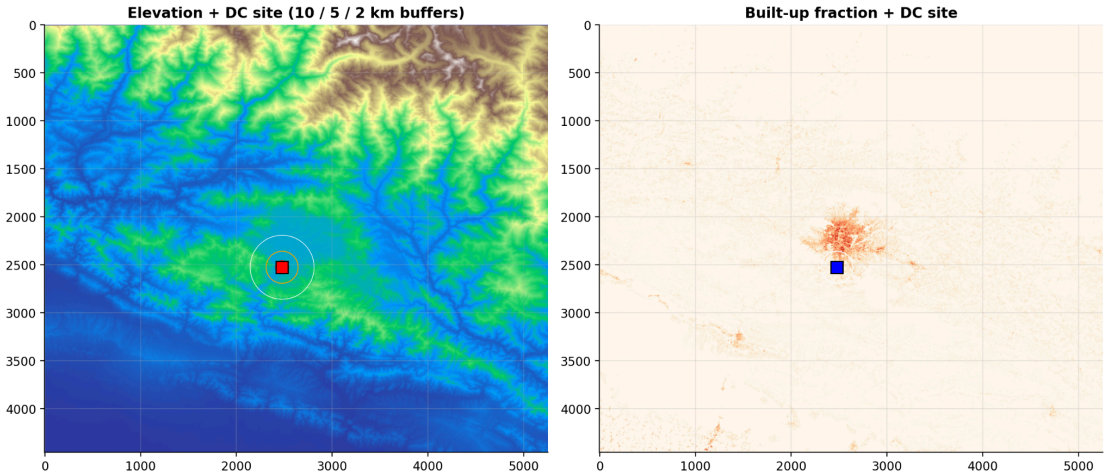

Figure 1. Hypothetical data center siting in the Kathmandu Valley. Left: SRTM 30 m elevation with the candidate site (red square) and 2 / 5 / 10 km buffers; central Kathmandu lies ~12 km north of the site. Right: GHSL 100 m built-up fraction over the same domain with the candidate site (blue square). The dense urban core is clearly displaced north of the candidate site along the valley axis.

3. Data and Methods

3.1 Datasets

Seven datasets were assembled, all clipped to a buffered Kathmandu Valley domain. ERA5-Land monthly reanalysis at 0.1° resolution for 2020 to 2024 (Muñoz-Sabater et al., 2021) provided 2 m air temperature, 2 m dewpoint, 10 m wind components, surface pressure, downward shortwave radiation, and total precipitation. MODIS Land Surface Temperature (MOD11A1, 1 km, April 2026) and Sentinel-2 NDVI (10 m, April 2026) provided contemporaneous surface state. ESA WorldCover (10 m, Zanaga et al., 2022) supplied land-cover classes; the Global Human Settlement Layer (GHSL) built-up surface product at 100 m (Pesaresi et al., 2024) supplied urban fraction. SRTM at 30 m (Farr et al., 2007) provided elevation, slope, and a valley-floor mask. Daily 2-m air temperature observations from Tribhuvan International Airport (TIA), spanning 2015 to 2025 (3,468 records), provided a single-point validation reference.

3.2 Anthropogenic heat flux

Three IT-load scenarios are defined: 50, 150, and 500 MW, corresponding respectively to a single traditional cloud data center (Barroso et al., 2013), a modern hyperscale AI training campus, and a frontier-AI build of the type currently being announced for North American sites (ABI Research, 2024). All scenarios assume a campus footprint of 20 ha, representative of contemporary land-banking and development targets for hyperscale facilities (Dgtl Infra, 2024), and a Power Usage Effectiveness (PUE) of 1.30, consistent with industry targets for modern air-cooled and hybrid designs. The campus-scale anthropogenic heat flux Q_F (W m^{-2}) is computed as:

$$Q_F = (P_{IT} \times PUE) / A_{campus}$$

where P_{IT} is the IT electrical load (W) and A_{campus} is the footprint area (m^2). The same total waste heat is also averaged onto a 1 × 1 km grid cell to produce the value that would be ingested by a mesoscale model, since direct injection at full campus density would be subgrid in any practical regional simulation. Following Sailor (2011) and the cooling-tower scheme of Wang et al. (2019), the total flux is partitioned into 70 percent sensible (Q_H) and 30 percent latent (Q_E) components, representing a hybrid air-plus-cooling-tower configuration. A diurnal multiplier representing the modulation of cooling load by ambient temperature is applied as a sinusoid with PUE varying from 1.20 (predawn) to 1.40 (afternoon peak).

3.3 Analytical plume model

Following Oke (1988) and the urban-plume scaling of Sailor (2011), the bulk near-surface temperature anomaly ΔT in the heat plume is approximated as:

$$\Delta T = (Q\_F \cdot L) / (\rho \cdot c\_p \cdot U \cdot h)$$

where L is the streamwise extent of the heat source (set to 1,000 m, the inner-domain grid scale), ρ is air density at valley elevation (1.10 kg m^{-3}), c_p is the specific heat of dry air at constant pressure (1,005 J kg^{-1} K^{-1}), U is the boundary-layer mean wind speed, and h is the mixing height. Two atmospheric regimes are evaluated: a well-mixed daytime regime with U = 3.5 m s^{-1} and h = 1,500 m, and a stable nocturnal valley regime with U = 1.5 m s^{-1} and h = 150 m. The latter values are within the range of nocturnal stable-layer parameters reported by Panday and Prinn (2009) for the Kathmandu Valley dry season, in which observations placed the cold-pool top at elevations consistent with mixing depths of order 100 to 400 m.

A complementary box model bounds the radiative-equilibrium ΔT under perfect nocturnal trapping by balancing waste-heat injection against Newtonian longwave cooling at coefficient $\lambda = 4\sigma T_0^3 \approx 5.4$ W m^{-2} K^{-1} (T_0 = 288 K), distributed over an effective valley-floor area A_v of 1.5×10^9 m^2. To test whether the steady-state plume formula remains valid in a closed valley where heat may accumulate overnight, we additionally developed a leaky-box model of the nocturnal cold-pool corridor (length 10 km × width 5 km × inversion depth 150 m, oriented along the drainage axis from the candidate site through central Kathmandu to the Bagmati gorge outlet). A two-dimensional Gaussian plume diagnostic is also computed for visualization purposes, with crosswind dispersion σ_y growing as $\sqrt{(1 + s/2{,}000)}$ for downwind distance s.

4. Results

4.1 Baseline climatology

The ERA5-Land 2020 to 2024 climatology recovers the canonical Kathmandu Valley annual cycle (Figure 2). Domain-mean 2 m temperature ranges from 7.6 °C in January to 20.5 °C in July; dewpoint depression peaks at ~10 K in April; total precipitation is concentrated in June to August (>15 mm/day daily mean during peak monsoon). Surface pressure averages 83.7 kPa, consistent with valley-floor elevation. Domain-mean 10 m wind speed remains below 0.65 m s^{-1} in all months, reflecting the cancellation of strong diurnal valley flows in the monthly mean and confirming the stagnation-prone nature of the synoptic background. Downward shortwave radiation peaks in April at 22.8 MJ m^{-2} day^{-1}, identifying the

pre-monsoon period as the maximum-insolation, minimum-precipitation window, with maximum sensitivity of the surface energy budget to local heat sources. The wind rose at the candidate site shows a southwest-dominated daytime resultant, consistent with the inflow regime documented by Regmi et al. (2003) through the Thankot pass and adjacent gaps.

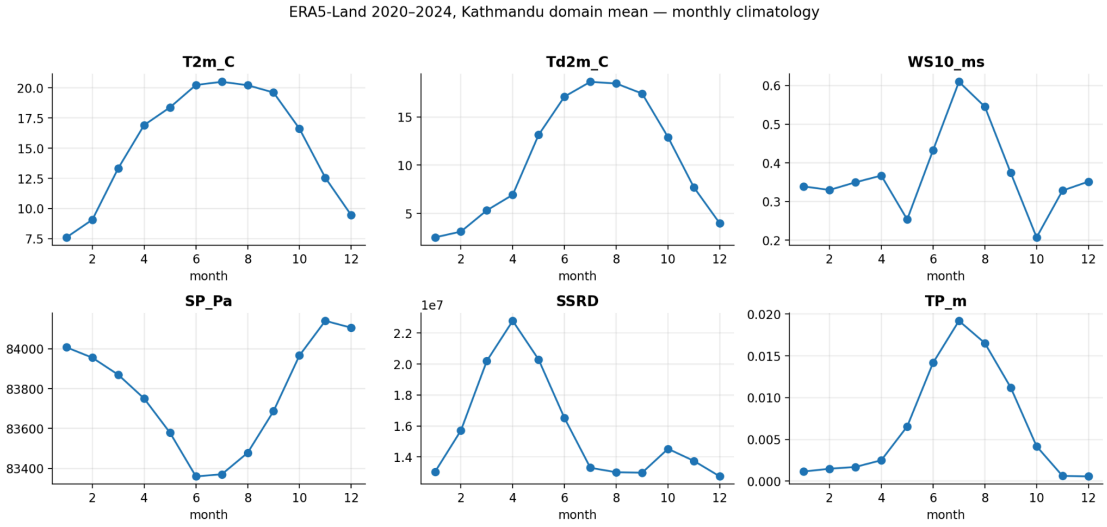

Figure 2. Domain-mean monthly climatology from ERA5-Land 2020 to 2024 over the Kathmandu Valley. Top row: 2 m air temperature, 2 m dewpoint, 10 m wind speed. Bottom row: surface pressure, downward shortwave radiation, total precipitation. April emerges as the pre-monsoon stagnation peak: maximum insolation, near-minimum precipitation, weak winds, large dewpoint depression.

4.2 Anthropogenic heat flux magnitudes

Computed AHF values span more than an order of magnitude across the three scenarios (Table 1, Figure 3). The 50 MW scenario, equivalent to a single traditional cloud facility, produces a campus-mean Q_F of 325 W m^{-2}, which is approximately 5× the intensity of the densest urban central business districts (CBDs) observed in high-resolution Asian urban datasets, where mean AHF typically ranges between 60 and 90 W m^{-2} (Sailor, 2011; Varquez et al., 2021). The 500 MW scenario, representing a frontier AI build, produces 3,250 W m^{-2}, a value that matches the diurnal peak of incident solar radiation at the surface but is sustained continuously. When averaged onto a 1 km mesoscale grid cell, these loads correspond to 65, 195, and 650 W m^{-2} respectively. These grid-cell values remain comparable to or exceed the citywide-mean AHF for the densest global megacities reported in current literature, such as the 50 to 75 W m^{-2} observed for the Pearl River Delta urban agglomeration (Wang et al., 2022) and the ~100 W m^{-2} localized peaks in modern South Asian industrial cores (Singh et al., 2025), with the critical distinction that the entire flux is concentrated within a single computational cell.

Table 1. Anthropogenic heat flux for each data center scenario at campus-local (20 ha) and 1 km mesoscale grid-cell scales.

Scenario	IT load (MW)	PUE	AHF campus (W m^{-2})	AHF on 1 km cell (W m^{-2})
Baseline (no DC)	0	1.00	0	0
Small (50 MW)	50	1.30	325	65
Medium (150 MW)	150	1.30	975	195
Large (500 MW)	500	1.30	3,250	650

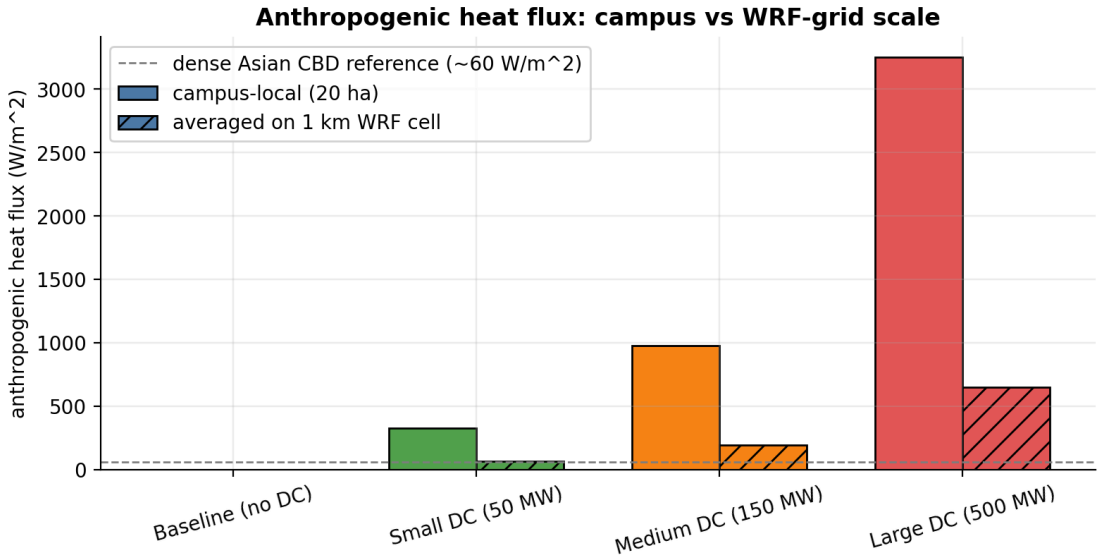

Figure 3. Anthropogenic heat flux per scenario at two spatial scales. Solid bars: campus-local AHF on the 20 ha footprint. Hatched bars: same total waste heat averaged onto a 1 km mesoscale grid cell. Dashed reference line: representative anthropogenic heat flux for dense Asian central business districts (~60 W m^{-2}, Sailor, 2011).

4.3 Analytical plume warming

The Oke-style plume model produces a strong day-night asymmetry in near-surface temperature anomaly (Table 2). For all three scenarios, the daytime regime gives ΔT below 0.12 °C, indistinguishable from background variability. The nocturnal regime produces ΔT of 0.26, 0.78, and 2.61 °C for the 50, 150, and 500 MW scenarios respectively, scaling linearly with Q_F as the model construction requires. The asymmetry factor between regimes is approximately 25, dominated by the collapse of mixing height from 1,500 m to 150 m and the reduction of wind speed from 3.5 to 1.5 m s^{-1}. Figure 4 places these regime points on a sensitivity sweep over the (U, h) parameter space.

Table 2. Analytical plume warming ΔT in the source grid cell at 1 km grid scale, for two representative atmospheric regimes.

Scenario	Regime	U (m s^{-1})	h (m)	ΔT (°C)
Small (50 MW)	Day, well-mixed	3.5	1,500	0.011
Medium (150 MW)	Day, well-mixed	3.5	1,500	0.034
Large (500 MW)	Day, well-mixed	3.5	1,500	0.112
Small (50 MW)	Night, stable valley	1.5	150	0.261
Medium (150 MW)	Night, stable valley	1.5	150	0.784
Large (500 MW)	Night, stable valley	1.5	150	2.613

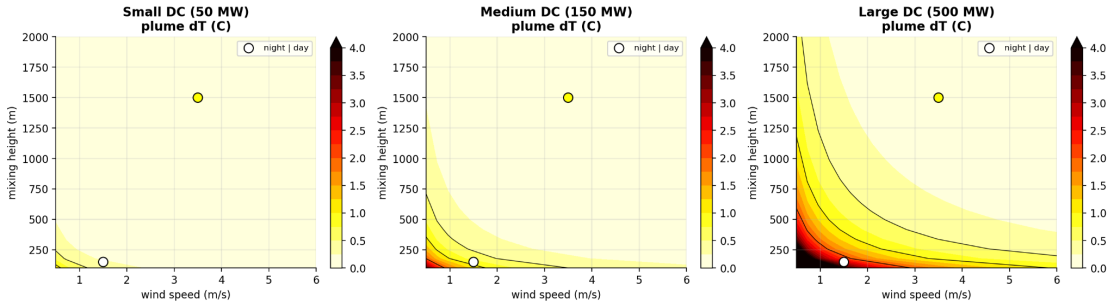

Figure 4. Sensitivity of source-cell plume ΔT to wind speed U and mixing height h across the three scenarios. Filled colour: ΔT (°C). Black contours: 0.5, 1, 2 °C iso-lines. Markers indicate the two representative regimes used in this study: white (nocturnal stable valley, U = 1.5 m s^{-1}, h = 150 m) and yellow (daytime well-mixed, U = 3.5 m s^{-1}, h = 1,500 m). Marker positions are identical across panels because atmospheric regime is independent of data center size; only the contour values change with IT load.

The radiative-equilibrium box model gives a complementary bound. The valley-mean ΔT under perfect nocturnal trapping ranges from 0.008 to 0.080 °C across the three scenarios, confirming that the spatially-distributed effect on the entire valley air mass is negligible. The notional campus-only equilibrium ΔT (60 to 600 °C) is unphysical and confirms that the system is ventilation-dominated rather than radiation-limited; the sensitivity sweep over (U, h) parameter space (Figure 4) shows that the 1 °C contour for the 150 MW scenario is reached only when U falls below 2 m s^{-1} and h below 400 m, conditions that coincide with the nocturnal stable layer documented by Panday and Prinn (2009).

The leaky-box analysis of nocturnal accumulation (Figure 6) demonstrates that the steady-state plume formula remains valid in this geometry. The combined relaxation timescale, set by advective drainage outflow ($\tau_{advect} \approx 1.9$ h at $U_{drainage} = 1.5$ m s^{-1}), longwave radiative cooling ($\tau_{rad} \approx 8.5$ h), and

weak nocturnal entrainment ($\tau_{ent} \approx 8.3$ h), is $\tau \approx 1.7$ hours, substantially shorter than a typical 8-hour stagnant night. The system therefore reaches near-equilibrium within the first ~3 hours after sunset and remains there until the convective breakup at sunrise. Multi-day stagnation episodes (5 to 7 consecutive nights) increase the corridor-mean dawn ΔT by only 10 to 30 percent through residual carryover under 50 percent daytime ventilation, well below the factor of 2 to 3 that significant accumulation would imply. We therefore report all subsequent quantitative thermal estimates against the source-cell value.

A separate and more practically important question is the warming experienced not at the data center but at the urban core, ~12 km north of the candidate site along the drainage axis. The Gaussian plume diagnostic, with crosswind dispersion $\sigma_y \approx 600 \cdot \sqrt{(1 + s/2{,}000)}$ and downwind distance s, predicts that the on-axis ΔT at central Kathmandu falls to approximately 15 to 40 percent of the source-cell value depending on the precise dispersion parameters. For the 150 MW medium scenario, this translates to an estimated urban-core nocturnal ΔT of 0.1 to 0.5 °C; for the 500 MW scenario, 0.4 to 2.0 °C. These values are an order of magnitude smaller than the existing surface UHI of 2 to 4 °C reported between dense and vegetation-rich wards in Kathmandu Metropolitan City (Bhandari & Zhang, 2022). The temperature signal of even a hyperscale data center, after accounting for plume dispersion across the 12 km between the candidate site and the urban core, is therefore modest in absolute terms relative to the city's existing thermal heterogeneity.

The two-dimensional Gaussian plume diagnostic illustrates the day-night asymmetry geometrically (Figure 5). Under the daytime up-valley regime, the plume is advected eastward and downward through the Bagmati gorge outlet, away from the urban core. Under the nocturnal drainage regime, the plume axis is oriented from the southern siting location toward central Kathmandu, with crosswind half-width of approximately 600 m at 5 km downwind, producing a narrow corridor of elevated ΔT over the densely-built central wards under the medium and large scenarios. The same urban wards are those identified by Bhandari and Zhang (2022) as having the highest priority for green-space mitigation due to their existing UHI severity.

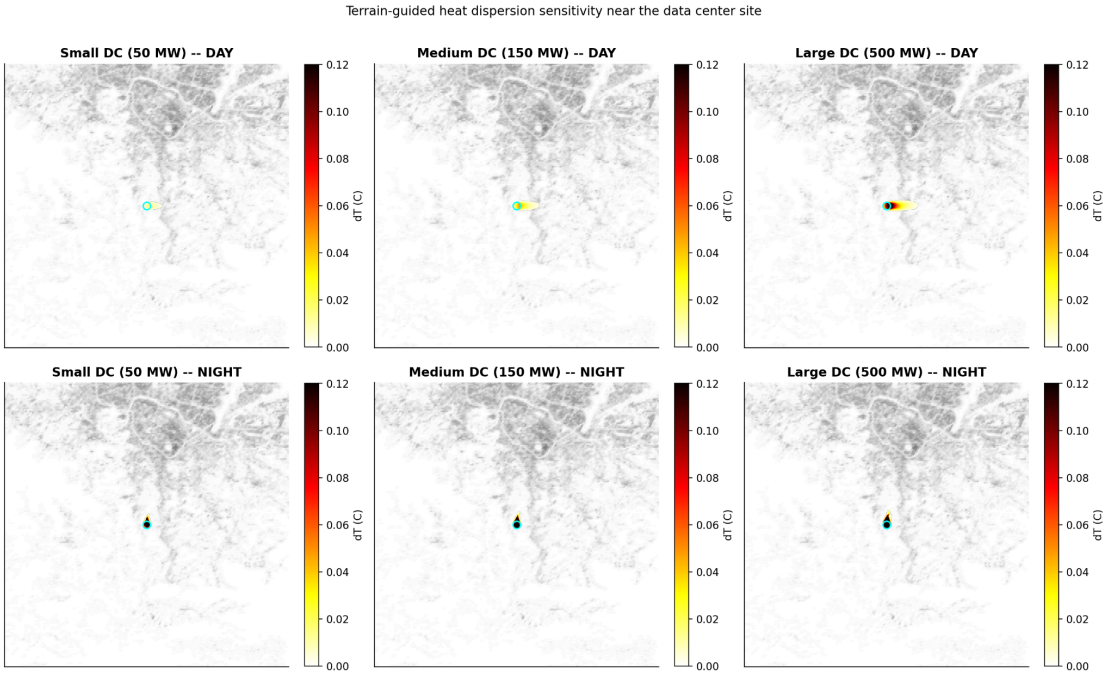

Figure 5. Spatial structure of the analytical plume warming for the three scenarios under daytime (top row) and nocturnal (bottom row) regimes. Cyan dot: data center site. Grey background: GHSL built-up fraction indicating the urban core to the north. Daytime up-valley flow advects the plume eastward, away from the city; nocturnal drainage carries the plume northward into central Kathmandu.

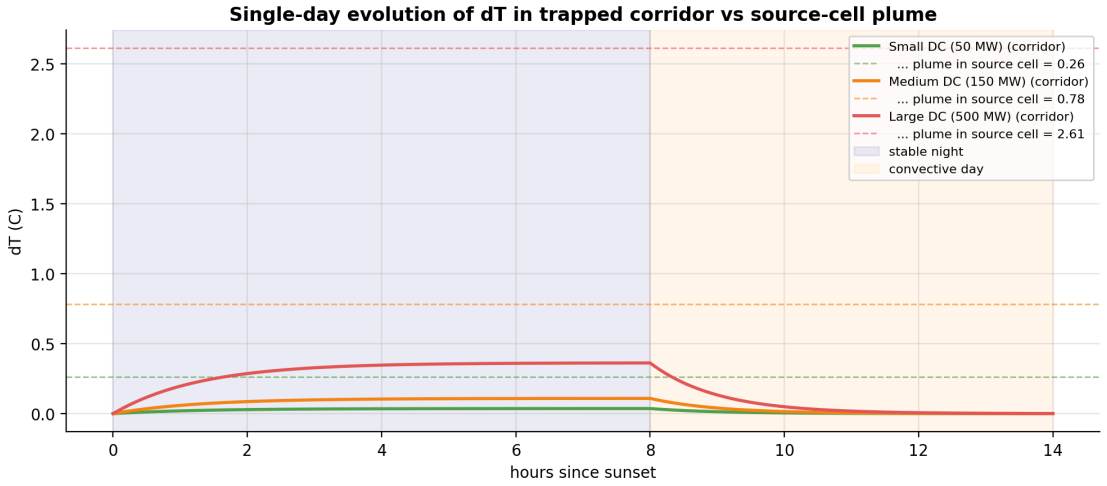

Figure 6. Single-night evolution of nocturnal ΔT in the cold-pool corridor for the three scenarios (solid lines), with the steady-state source-cell plume values shown as dashed reference lines. Stable-night accumulation reaches equilibrium within ~3 hours of sunset and remains there until convective breakup at sunrise (vertical regime shading). The corridor-mean ΔT remains well below the source-cell ΔT because the corridor (50 km²) is much larger than the source cell (1 km²); the time-integrated calculation confirms that the steady-state formula provides the correct order of magnitude.

5. Discussion

5.1 The signal is local, nocturnal, and regime-dependent

Our analytical results indicate that the dominant near-surface temperature impact of a hypothetical hyperscale data center on the southern Kathmandu Valley floor is concentrated in a narrow plume (crosswind extent of order 1 km, Figure 5), oriented along the nocturnal drainage axis toward the urban core, and active primarily during the stable-boundary-layer hours of approximately 21:00 to 06:00 local time. For the medium scenario (150 MW), the source-cell ΔT is 0.78 °C and the dispersed urban-core ΔT is 0.1 to 0.5 °C; for the large scenario, 2.61 °C and 0.4 to 2.0 °C respectively. The valley-average effect is negligible across all scenarios. This pattern is consistent with the general finding that anthropogenic heat (Q_F) strongly affects nocturnal temperature in stable boundary layers but has a weak influence on daytime well-mixed conditions (Kusaka et al., 2012; Li et al., 2024). It is also consistent with observations in studies of Asian valley and basin cities, which demonstrate that industrial-scale Q_F affects the diurnal cycle most intensely during stagnation events when horizontal ventilation is suppressed (Wang et al., 2022; Doan et al., 2023). Furthermore, the high sensitivity of nocturnal temperatures to Q_F in industrial zones has been verified in numerical experiments where a significant industrial heat island emerges only after sunset, as the shallow stable boundary layer traps waste heat near the surface (Mishra & Kannan, 2022).

5.2 Magnitude relative to existing heterogeneity

After accounting for plume dispersion across the 12 km fetch between the candidate site and the urban core, the analytical estimate of nocturnal warming at central Kathmandu is 0.1 to 0.5 °C for the 150 MW scenario. This is an order of magnitude smaller than the surface UHI of 2 to 4 °C that the city already experiences due to existing land-use patterns (Bhandari & Zhang, 2022). For the 50 MW scenario, the urban-core ΔT falls below 0.05 °C, a value essentially indistinguishable from the background meteorological noise and internal variability of the valley's boundary layer (Sun et al., 2021). However, the 500 MW scenario, with an urban-core ΔT of 0.4 to 2.0 °C, produces a temperature signature comparable in magnitude to the existing UHI gradient, making it clearly detectable against background variability. The relationship between facility size and local climate impact is therefore characterized by a detection threshold rather than a simple linear progression: while small-to-medium facilities remain atmospherically benign due to dispersive dilution, frontier-scale builds cross a critical threshold where their thermal footprint becomes a significant component of the urban climate (Mishra & Kannan, 2022; Varquez et al., 2021).

5.3 Co-incidence with existing air-quality and inversion stress

A finding that does not fall out of any single dataset but emerges from juxtaposition with the published air-quality literature is that the hours and seasons of maximum thermal impact identified here coincide with the hours and seasons of the Kathmandu Valley's worst air-quality episodes. PM2.5 in the valley reaches its highest levels during the late-night-to-morning hours of January to April, when stable inversions trap pollutants from cookstoves, vehicles, and brick kilns near the surface (Mues et al., 2017; Saud & Paudel, 2018; IQAir, 2023). The same inversion regime is responsible for the elevated ΔT we find in our nocturnal plume calculation. The two effects therefore stack: the data center plume is largest precisely when the cold-pool ventilation deficit is most severe. Our analytical model does not resolve interactions with chemistry, and we make no claim about chemical transformation; but the meteorological coincidence is robust and worth noting because ground-level impacts on residents would experience them simultaneously rather than independently.

5.4 Limitations

Several limitations should be acknowledged. First, the analytical plume model is a steady-state, single-source Gaussian formulation and does not capture vertical entrainment, convective overturning at high Q_F values, or interaction with the existing urban canopy. The source-cell 2.61 °C value reported for the 500 MW scenario is an upper bound at the data center itself; the dispersed urban-core estimate of 0.4 to 2.0 °C accounts for plume falloff but does not capture convective overturning, which would further cap the high-Q_F response. A higher-fidelity mesoscale simulation would be required to quantify these corrections.

Second, our nocturnal regime parameters ($U = 1.5$ m s^{-1}, $h = 150$ m) are chosen to be representative but were not derived from observations specific to the candidate site. The ERA5-Land monthly winds at the site (annual mean 0.37 m s^{-1}) reflect the cancellation of diurnal valley flows in monthly means, not actual nocturnal drainage speeds; published in-situ observations from Panday and Prinn (2009) report nocturnal drainage winds of 0.5 to 3 m s^{-1} at various Kathmandu Valley sites depending on slope geometry. Selecting a smaller U would increase the nocturnal ΔT roughly inversely; the magnitude estimates in Table 2 should therefore be understood as a moderate point in a 1.5 to 4× uncertainty range, with the upper end being more pessimistic for impacts on the city.

Third, the assumption that 100 percent of IT power emerges as low-grade heat at the campus surface is the standard energy-balance assumption (Sailor, 2011), but in practice the heat exits at varying heights depending on cooling-tower stack geometry. Most urban-canopy schemes treat anthropogenic heat as a near-surface flux, which biases any subsequent model response toward the surface layer. A more

accurate treatment would require either an elevated point-source representation or post-processing of plume rise from a Briggs-style formulation (Briggs, 1975).

Fourth, the satellite snapshots used for surface state (NDVI, LST) are from April 2026, while the climatological baseline draws from 2020 to 2024. Inter-annual variability in vegetation cover and surface temperature is non-negligible in this region; using contemporaneous snapshots would be preferable but is constrained by the cloud-cover-free imagery available. The choice of the April pre-monsoon window for analysis is justified by the stagnation regime characterizing the period; other windows (notably the deep-winter inversion period of December to February) might produce stronger nocturnal trapping and warrant separate analysis in follow-up work.

Fifth, the 500 MW scenario, while now within the announced design range for North American AI campuses (MMCG Invest, 2026), is not realistic for Kathmandu under current grid conditions: Nepal's national peak demand is approximately 2 GW, and the valley's 220 kV transmission ring has limited spare capacity (Nepal Electricity Authority, 2024). The 500 MW result should therefore be read as a thought experiment that bounds the consequences of the upper end of currently-deployed AI infrastructure if it were placed in this geography, rather than as a forecast of any specific project.

Finally, this study is restricted to the atmospheric dimension of data center siting and does not evaluate the water demand of evaporative cooling, the regional energy-grid implications of hyperscale electrical loads, or the chemistry of the heat plume in interaction with the valley's existing pollutant burden. The water demand in particular is expected to be the binding non-atmospheric constraint, given the Kathmandu Valley's documented dry-season water deficit and groundwater drawdown (Thapa et al., 2019; Pandey et al., 2020), and we recommend a dedicated hydrological assessment as a prerequisite for any policy decision on large-scale data center approval. The framework presented here addresses the atmospheric component of that broader evaluation.

5.5 Generalizability

The findings here, while specific to Kathmandu, are not unique to it. Topographically similar bowl-shaped valley cities exist throughout South and Central Asia (Salt Lake City, Mexico City, Santiago, Tehran, Kabul, Lhasa, parts of Quito), and several share Kathmandu's combination of stagnation-prone boundary layer and monsoonal precipitation regime. The qualitative result that hyperscale data center siting in such cities produces a localized nocturnal heat plume that is small for small facilities and detectable for large ones likely generalizes. The specific magnitudes will differ depending on valley geometry, prevailing wind

regime, and local meteorological conditions; the framework presented here can be applied to any such city using equivalent ERA5-Land, MODIS, and GHSL datasets.

6. Conclusions

This study presents a quantitative analytical assessment of the meteorological implications of a hypothetical data center sited in the Kathmandu Valley. We find:

(1) Daytime urban-core temperature anomaly is below 0.1 °C across all three IT-load scenarios (50, 150, and 500 MW), because the prevailing up-valley flow ventilates the heat plume away from the city.

(2) Nocturnal warming under the valley's stable boundary layer reaches 0.26, 0.78, and 2.61 °C respectively in the 1 km grid cell directly above the data center site. After accounting for plume dispersion across the ~12 km distance to the urban core, the central-Kathmandu ΔT is estimated at < 0.05, 0.1 to 0.5, and 0.4 to 2.0 °C respectively. Time-integrated box-model analysis confirms that the steady-state plume formula remains valid because the cold-pool advective relaxation timescale (~1.7 h) is short compared to the typical stagnant-night length (~8 h); accumulation does not change the order of magnitude.

(3) The dependence on facility size is not linear in practical-impact terms. A small data center on the order of 50 MW is of limited meteorological concern under the valley's stagnation regime, producing urban-core temperature anomalies indistinguishable from background variability. Larger facilities cross the threshold at which their thermal footprint becomes measurable against the existing urban heat island, with the 500 MW scenario producing a temperature signature comparable in magnitude to the existing UHI gradient.

(4) The thermal impact at the urban core is therefore bounded by valley meteorology and falls within the range that established urban-climate management tools can address. The atmospheric dimension is not, in itself, a decisive barrier to small or medium data center siting in the valley.

(5) The decisive remaining uncertainty is non-atmospheric. The water demand of evaporative cooling at hyperscale loads has the potential to interact with the valley's existing dry-season water deficit, and this dimension must be quantified through dedicated hydrological assessment before any large-scale data center development is approved at the policy level.

These findings indicate that the atmospheric signal of a hyperscale data center in the Kathmandu Valley is small for small facilities and modest for large ones, while the decisive constraint for policy purposes lies in the water and energy dimensions that fall outside the present analysis. Future work should prioritize the hydrological and grid-capacity assessments needed to evaluate large-scale facility siting in this geography.

Acknowledgements

The author thanks the Department of Hydrology and Meteorology, Government of Nepal, for access to TIA station observations; ICIMOD for ground-truth reference datasets; and ECMWF, NASA, and ESA for the ERA5-Land, MODIS, and Sentinel-2 / WorldCover archives respectively. All datasets used are publicly available.

Data Availability

All code used to generate the figures and tables in this paper, including the analytical plume model and the anthropogenic-heat-flux raster generator, is archived in the project's repository. ERA5-Land monthly data are available from the Copernicus Climate Data Store. MODIS LST is available from NASA LP DAAC. Sentinel-2 imagery and ESA WorldCover are available through the Copernicus Open Access Hub. SRTM DEM is available from USGS Earth Explorer. GHSL built-up products are available from the European Commission JRC.

Declaration of Generative AI Use

Generative AI tools were used to assist with language refinement, editing, and organizational structuring during manuscript preparation. All scientific analysis, interpretation, and final content were reviewed and verified by the author.

References

ABI Research. (2024). Hyperscale data center infrastructure and AI training loads. ABI Research Market Data Reports.

Attenni, G., Arroba, P., Moreno-Vozmediano, R., & Risco-Martín, J. L. (2026). Spatio-temporal shifting to reduce carbon, water, and land-use footprints of cloud workloads. arXiv. https://arxiv.org/abs/2512.08725

Barroso, L. A., Clidaras, J., & Hölzle, U. (2013). The datacenter as a computer: An introduction to the design of warehouse-scale machines (2nd ed.). Morgan & Claypool Publishers.

Bhandari, S., & Zhang, C. (2022). Urban green space prioritization to mitigate air pollution and the urban heat island effect in Kathmandu Metropolitan City, Nepal. Land, 11(11), 2074. https://doi.org/10.3390/land11112074

Briggs, G. A. (1975). Plume rise predictions. In Lectures on air pollution and environmental impact analyses (pp. 59–111). American Meteorological Society.

Chen, S., & Hu, D. (2017). Parameterizing anthropogenic heat flux with an energy-consumption inventory and multi-source remote sensing data. Remote Sensing, 9(11), 1165. https://doi.org/10.3390/rs9111165

Dgtl Infra. (2024). Data center footprint and land development trends. Digital Infrastructure Analysis. https://dgtlinfra.com/hyperscale-and-hyperscalers/

Doan, V. Q., Kusaka, H., Sato, T., & Chen, F. (2023). Impact of urbanization on the local climate of rapidly growing Asian megacities: A case study of tropical stagnation events. Urban Climate, 49, 101482.

Farr, T. G., Rosen, P. A., Caro, E., Crippen, R., Duren, R., Hensley, S., … Alsdorf, D. (2007). The Shuttle Radar Topography Mission. Reviews of Geophysics, 45(2), RG2004.

Hu, D., Yang, L., Zhou, J., & Deng, L. (2012). Estimation of urban energy heat flux and anthropogenic heat discharge using ASTER image and meteorological data: Case study in Beijing metropolitan area. Journal of Applied Remote Sensing, 6(1), 063559. https://doi.org/10.1117/1.JRS.6.063559

IQAir. (2023). 2023 World Air Quality Report.

Kusaka, H., Chen, F., Tewari, M., Dudhia, J., Gill, D. O., Duda, M. G., Wang, W., & Miya, Y. (2012). Numerical simulation of urban heat island effect by the WRF model with 4-km grid increment: An inter-comparison study between the urban canopy model and slab model. Journal of the Meteorological Society of Japan, 90B, 33–45.

Lawson, S., Cooke, C., Ryken, A., Cooper, B., & Margulis, S. (2026). Data center expansion in Virginia: Closing critical gaps for informed water planning and permitting. Illinois Secure Water Initiative. https://securewater.illinois.edu/data-center-expansion-in-virginia-closing-critical-gaps-for-informed-water-planning-and-permitting/

Li, Y., Chen, F., Barlage, M., & Tewari, M. (2024). Structural uncertainty in the sensitivity of urban temperatures to anthropogenic heat flux. Journal of Advances in Modeling Earth Systems, 16(10). https://doi.org/10.1029/2024MS004245

Mahata, K. S., Rupakheti, M., Haslett, S. L., Ali, K., Safai, P. D., Ohmura, A., … Lawrence, M. G. (2017). Seasonal and diurnal variations in methane and carbon dioxide in the Kathmandu Valley in the foothills of the central Himalayas. Atmospheric Chemistry and Physics, 17(17), 10473–10493. https://doi.org/10.5194/acp-17-10473-2017

Mishra, S. K., & Kannan, R. (2022). The effect of anthropogenic heat and moisture on local weather at industrial heat islands: A numerical experiment. Atmosphere, 13(3), 357. https://doi.org/10.3390/atmos13030357

MMCG Invest. (2026, March 15). AWS at scale: Inside the largest private infrastructure buildout the world has ever seen. https://www.mmcginvest.com/post/aws-at-scale-inside-the-largest-private-infrastructure-buildout-the-world-has-ever-seen

Morgan, T. P. (2014). A rare peek into the massive scale of AWS. The Next Platform / EnterpriseAI.

Mues, A., Rupakheti, M., Münkel, C., Lauer, A., Bozem, H., Hoor, P., … Lawrence, M. G. (2017). Investigation of the mixing layer height derived from ceilometer measurements in the Kathmandu Valley and implications for local air quality. Atmospheric Chemistry and Physics, 17(13), 8157–8176. https://doi.org/10.5194/acp-17-8157-2017

Muñoz-Sabater, J., Dutra, E., Agustí-Panareda, A., Albergel, C., Arduini, G., Balsamo, G., … Thépaut, J.-N. (2021). ERA5-Land: A state-of-the-art global reanalysis dataset for land applications. Earth System Science Data, 13(9), 4349–4383.

Nepal Electricity Authority. (2024). NEA annual report 2023/24. Kathmandu, Nepal.

Oke, T. R. (1988). The urban energy balance. Progress in Physical Geography, 12(4), 471–508.

Panday, A. K., & Prinn, R. G. (2009). Diurnal cycle of air pollution in the Kathmandu Valley, Nepal: Observations. Journal of Geophysical Research: Atmospheres, 114, D09305.

Pandey, V. P., Shrestha, S., & Kazama, F. (2020). Implications of the Melamchi water supply project for the Kathmandu Valley groundwater system. Water Policy, 21(S1), 120–137.

Pesaresi, M., Politis, P., Florczyk, A. J., Schiavina, M., Freire, S., Maffenini, L., … Sabo, F. (2024). GHS-BUILT-S: Global built-up surface from Sentinel-2 (R2023A). European Commission, Joint Research Centre.

Regmi, R. P., Kitada, T., & Kurata, G. (2003). Numerical simulation of late wintertime local flows in Kathmandu Valley, Nepal: Implication for air pollution transport. Journal of Applied Meteorology, 42(4), 389–403.

Sailor, D. J. (2011). A review of methods for estimating anthropogenic heat and moisture emissions in the urban environment. International Journal of Climatology, 31(2), 189–199. https://doi.org/10.1002/joc.2106

Saud, B., & Paudel, G. (2018). The threat of ambient air pollution in Kathmandu, Nepal. Journal of Environmental and Public Health, 2018, 1504591. https://doi.org/10.1155/2018/1504591

Shakya, K. M., Peltier, R. E., Shrestha, H., & Byanju, R. M. (2017). Measurements of TSP, PM10, PM2.5, BC, and PM chemical composition from an urban residential location in Nepal. Atmospheric Pollution Research, 8(6), 1123–1131. https://doi.org/10.1016/j.apr.2017.05.002

Singh, R., Kumar, A., & Sharma, P. (2025). Impact of rapid industrialization on anthropogenic heat flux and urban boundary layers in semi-arid environments. Atmospheric Research, 312, 107–124.

Sun, T., Wang, Z. H., Grimmond, C. S. B., Yang, J., Ward, H. C., Kotthaus, S., … Lipson, M. (2021). Ten questions concerning the modelling of anthropogenic heat in the urban boundary layer. Building and Environment, 196, 107792.

Synergy Research Group. (2024). Hyperscale data center count hits 1,136. Industry brief.

Thapa, B. R., Ishidaira, H., Pandey, V. P., & Shakya, N. M. (2019). Implications of the Melamchi water supply project for the Kathmandu Valley groundwater system. Water Policy, 21(S1), 120–137.

Turkay, B. M., Pehlivan, I., Onat, N. C., Kucukvar, M., & Türkay, M. (2026). Scenario-based forecasting of the global energy demand and carbon footprint of artificial intelligence. PLOS One, 21(3), e0343056. https://doi.org/10.1371/journal.pone.0343056

Varquez, A. C. G., Kiyomoto, S., Khan, M. S., & Kanda, M. (2021). Global 1-km long-term annual anthropogenic heat flux dataset with regional and fuel-type variations. Scientific Data, 8(1), 1–13. https://doi.org/10.1038/s41597-021-01050-3

Wang, C., Wang, Z. H., & Yang, J. (2022). Localized urban canopy model and improved anthropogenic heat parameters: Simulation of warm-sector heavy rainfall over the Pearl River Delta. Frontiers in Environmental Science, 10, 1078820. https://doi.org/10.3389/fenvs.2022.1078820

Wang, J., Feng, J., Yan, Z., & Chen, Y. (2019). On the assessment of a cooling tower scheme for high-resolution numerical weather modeling for urban areas. Journal of Applied Meteorology and Climatology, 58(6), 1229–1245. https://doi.org/10.1175/JAMC-D-18-0126.1

Zanaga, D., Van De Kerchove, R., Daems, D., De Keersmaecker, W., Brockmann, C., Kirches, G., … Arino, O. (2022). ESA WorldCover 10 m 2021 v200. https://doi.org/10.5281/zenodo.7254221